Alpha Heating and Burning Plasmas in Inertial Confinement Fusion

R. Betti,[1] A. R. Christopherson,[1] B. K. Spears,[2] R. Nora,[2] A. Bose,[1] J. Howard,[1] K. M. Woo,[1] M. J. Edwards,[2] and J. Sanz[3]

[1]*Fusion Science Center and Laboratory for Laser Energetics, University of Rochester, Rochester, New York 14623, USA*

[2]*Lawrence Livermore National Laboratory, Livermore, California 94550, USA*

[3]*Universidad Politcnica de Madrid, Madrid 28040, Spain*

(Received 1 April 2015; published 26 June 2015)

Estimating the level of alpha heating and determining the onset of the burning plasma regime is essential to finding the path towards thermonuclear ignition. In a burning plasma, the alpha heating exceeds the external input energy to the plasma. Using a simple model of the implosion, it is shown that a general relation can be derived, connecting the burning plasma regime to the yield enhancement due to alpha heating and to experimentally measurable parameters such as the Lawson ignition parameter. A general alpha-heating curve is found, independent of the target and suitable to assess the performance of all laser fusion experiments whether direct or indirect drive. The onset of the burning plasma regime inside the hot spot of current implosions on the National Ignition Facility requires a fusion yield of about 50 kJ.

DOI: 10.1103/PhysRevLett.114.255003 PACS numbers: 52.57.Bc, 28.52.Cx, 52.55.Pi, 52.57.Fg

In inertial confinement fusion [1] (ICF) a shell of cryogenic deuterium and tritium (DT) ice is imploded at high velocities (300–400 km/s) and low entropy to achieve high central temperatures and high areal densities [2]. The final fuel assembly consists of a relatively low-density (30–100 g/cc), high-temperature (5–10 keV) core—the hot spot—surrounded by a dense (300–1000 g/cc), cold (200–500 eV) fuel layer—the compressed shell. Fusion alphas are produced from the D + T fusion reactions with an energy $\varepsilon_\alpha = 3.5$ MeV and slow down primarily through collisions with the plasma electrons. The alpha-heated electrons transfer part of their energy to the D and T ions thus increasing the fusion reaction rate. The process of alpha energy deposition to the hot spot of a compressed ICF capsule is called *alpha heating*. Ignition is a direct consequence of alpha heating and of its feedback on the thermal energy and fusion reaction rate. When this feedback process becomes unstable, it leads to a thermal runaway within the central hot spot [2]. A robustly ignited hot spot drives a burn wave in the surrounding dense shell leading to fusion energy outputs in the megajoule range greatly exceeding the thermal and kinetic energy supplied to the DT fuel by the implosion alone (~ tens of kilojoules).

Recent experiments at the National Ignition Facility (NIF) (High-Foot targets [3]) have demonstrated significant alpha heating using indirect drive (ID). To make progress towards ignition at the NIF [4], it is crucial to be able to measure the level of alpha heating and to identify intermediate plasma states where the alpha heating is the leading source of input energy (alpha dominated or burning plasmas). In magnetic confinement fusion (MCF) [5], the burning plasma regime is identified through the thermonuclear $Q =$ fusion power output/external power input. Since the alpha energy is about 1/5 of the total fusion energy, a $Q = 5$ denotes the state where the alpha power equal the input power. For convenience, in this Letter we use $Q_\alpha =$ alpha power/input power $= Q/5$ and define the onset of a burning plasma at $Q_\alpha = 1$ ($Q = 5$).

While determining Q_α for a steady state MCF device is straightforward, the definition for ICF is greatly complicated by the transient nature of an ICF implosion and by the fact that the vast majority of the input energy does not reach the DT plasma. Since this Letter is only concerned with the physics of burning plasmas and not with the prospects for fusion energy, the relevant input energy is the one reaching the DT plasma where the fusion reactions occur. Therefore, the parameters Q, Q_α used here refer to the DT fuel and should not be confused with the engineering Q used for fusion reactors [5].

Heating by the alphas enhances the fusion yield to varying degrees depending on the fraction of deposited alpha particle energy to the total hot spot energy. In this Letter, we consider yield amplifications $\lesssim 10$ that are of most interest for current implosions on the NIF and characteristic of a subignited burning plasma. Using a simple model of the hot spot and shell dynamics (*alpha heating model*), we find the burning-plasma conditions for ICF and show that the fusion yield enhancement due to alpha heating depends only on the Lawson parameter [6,7] through a universal curve valid for direct and indirect drive ICF. It is shown that the alpha-heating model results agree with radiation-hydrodynamics simulations.

The alpha heating model describes both the hot spot formation and the piston action of the shell providing the external input energy. To correctly capture the pdV work to the hot spot and to the shell, the incompressible shell model [7] is not suitable, instead a compressible model similar to the one in [8] is used. In the final stage of the implosion, the

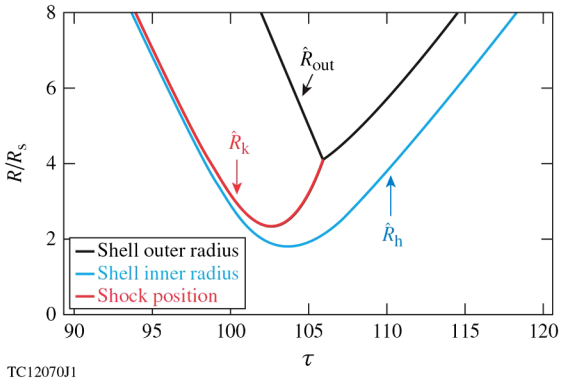

FIG. 1 (color online). Trajectories from the model (1)–(5) using $\beta = 0$, $\gamma = 0$. The figure shows the time evolution of the hot spot radius, the return shock inside the shell and the shell outer surface.

shell is described as a compressible gas separated into two regions (shocked and free-fall) by the return or rebound shock driven by the hot spot pressure into the shell. The temporal evolution of the hydrodynamic quantities is determined from the beginning of the shell deceleration phase up to the shell rebound, and both the heat conduction and radiation losses are included. A fraction of the alpha particles escapes through the hot spot boundary, depositing its energy into the cold shell and ablating shell mass into the hot spot. It is assumed that all radiation escapes from the hot spot reducing the pressure and temperature. The fusion rate is approximated with $\langle\sigma v\rangle \sim c_\alpha T^3$ ($c_\alpha = \text{const}$), which is sufficiently accurate in the interesting range 4–8 keV, characteristic of a yield amplification ≤ 10. The conservation equations for mass, momentum, and energy can be written in the dimensionless form

$$(\hat{P}\hat{R}_h^3/\hat{T})' = \hat{R}_h\hat{T}^{5/2} + 3/5(1-\theta_\alpha)\gamma\hat{p}^2\hat{R}_h^3, \quad (1)$$

$$(\hat{M}_{ss}\hat{U}_{ss})' - \dot{\hat{M}}_{ss}\hat{U}_{ff}(\hat{R}_k) = \hat{P}\hat{R}_h^2 + 2\int_{\hat{R}_h}^{\hat{R}_k}\hat{r}\hat{P}_{ss}d\hat{r}, \quad (2)$$

$$\dot{\hat{M}}_{ss} = \hat{R}_k^2\hat{\rho}_{ff}(\hat{R}_k)(\dot{\hat{R}}_k - \hat{U}_{ff}), \quad (3)$$

$$\dot{\hat{R}}_k = 4/3\hat{U}_{ss}(\hat{R}_k) - 1/3\hat{U}_{ff}(\hat{R}_k), \quad (4)$$

$$(\hat{P}\hat{R}_h^5)' = \hat{P}^2\hat{R}_h^5(\gamma\hat{T} - \beta\hat{T}^{-3/2}). \quad (5)$$

The first is the hot spot mass conservation used to infer the hot spot temperature T with the right-hand side representing the mass ablation off the inner shell surface driven by the heat conduction [7] and alpha particle losses [9]. Here, $\hat{R}_h$ represents the hot spot radius. The second equation represents Newton's law for the shocked portion of the shell slowed down by the hot spot pressure P. The return shock R_k separates the free-fall (ff) and the shocked (ss) regions of the shell. The shocked shell pressure P_{ss} varies linearly from the hot spot pressure to the post-shock pressure given by the Rankine-Hugoniot (RH) relations. The third equation governs the shocked-shell mass and includes the flow of mass across the return shock. The fourth equation describes the evolution of the return shock position R_k through the RH relations. The velocity within the shocked shell is determined through a Taylor expansion from the hot spot radius using the isentropic relation of the shocked shell leading to

$$\hat{U}_{ss}(\hat{r}) \approx \dot{\hat{R}}_h + [\dot{\hat{R}}_h/\hat{R}_h - (3/5)\dot{\phi}/\phi](\hat{r} - \hat{R}_h), \quad (6)$$

where $\phi \equiv \hat{P}\hat{R}_h^5$. Equation (5) is the hot spot energy conservation where the two terms on the right-hand side represent the alpha heating contribution and the radiation losses. Pressure, radius, and temperature are normalized with their stagnation values T_s, P_s, R_s in the absence of alpha heating and radiation losses, and for an incompressible shell with equal mass,

$$M_{sh}V_i^2 = 4\pi P_s R_s^3, \quad (7)$$

$$\kappa_0 T_s^{7/2} \approx P_s R_s V_i, \quad (8)$$

where V_i is the implosion velocity, M_{sh} is the shell mass and κ_0 is the Spitzer thermal conductivity coefficient [10] in $\kappa_{Sp} = \kappa_0 T^{5/2}$. In the ideal hot-spot plasma, Spitzer conduction is a valid approximation [11]. The dimensionless time is $\tau = tV_i/R_s$. The dimensionless velocity is normalized with the peak implosion velocity V_i. For simplicity, we assume an initially uniform velocity profile so that $\hat{U}_{ff} = -1$. The dimensionless shocked-shell mass is defined as $\hat{M}_{ss} = M_{ss}/M_{sh}$. The dimensionless shell density is defined as $\hat{\rho} = \rho/(M_{sh}/4\pi R_s^3)$ and its profile during the coasting phase (or free fall) is assumed approximately parabolic. The constant $\gamma \approx c_\alpha\varepsilon_\alpha P_s T_s R_s/(24V_i)$ determines the level of alpha heating. The parameter $\beta \approx c_b P_s R_s/(6T_s^{3/2}V_i)$ determines the radiation losses (c_b is the bremsstrahlung constant for the radiated power density $\dot{P}_{rad} \approx c_b n^2\sqrt{T}$). Some three dimensional effects due to the reduction of the hot spot volume [12] from the deceleration-phase Rayleigh-Taylor spikes can be included through a clean volume analysis as described in Ref. [7] but are omitted for simplicity in this Letter. The fraction of escaping alphas is determined using Ref. [13]:

$$\theta_\alpha(\xi_\alpha > 1/2) = 1 - 1/(4\xi_\alpha) + 1/(160\xi_\alpha^3), \quad (9)$$

$$\theta_\alpha(\xi_\alpha < 1/2) = 3/2\xi_\alpha - 4/5\xi_\alpha^2, \quad (10)$$

where $\xi_\alpha = \xi_0\hat{P}\hat{R}/\hat{T}^{5/2}$. We use $\xi_0 = 0.6$ leading to a fraction of absorbed alphas at bang time of about 0.7–0.8 in agreement with numerical simulations including alpha

transport physics. Equations (1)–(5) are solved from the beginning of the deceleration phase ($t = 0$) with a radius much greater than the stagnation radius $\hat{R}_h(0) = \hat{R}_0 \gg 1$, velocity equal to the implosion velocity $\dot{\hat{R}}_h(0) = -1$, very low initial pressure and temperature $\hat{P}(0) = \hat{R}(0)^{-5/2}$, $\hat{T}(0) = \hat{R}(0)^{-1/2}$. At $t = 0$, the return shock is approaching the imploding shell $[\hat{R}_k(0) = \hat{R}_0]$ and the shocked shell mass is zero $[\hat{M}_{ss}(0) = 0]$. The initial aspect ratio is set to $A_0 \approx 0.1\hat{R}_h(0)$ leading to a stagnating mass of about 50% of the DT unablated mass as indicated by hydrodynamic simulations of ignition targets [7]. Figure 1 shows the trajectories of the inner shell surface (or hot spot radius), return shock, and outer shell surfaces. After the return shock reaches the outer surface, the entire shell mass is shocked and the shell behaves like a rigid piston.

The solution of Eqs. (1)–(5) exhibits a singularity (ignition) for a critical value of γ that depends on β. A numerical solution leads to the critical $\gamma(\beta) \approx 28 + 4.3\beta + 2\beta^2$ for $\beta \leq 2$. The ignition parameter can be written as $\chi_{no\alpha} = \gamma/\gamma(\beta)$ with $\chi_{no\alpha} = 1$ being the ignition condition. From full hydrodynamic simulations with radiation on or off, we determine that radiation losses cause a reduction of about 15%–20% in hot spot pressure and temperature corresponding to a value of $\beta \approx 1.5$ in the model (1)–(5). The subscript $no\alpha$ indicates that all the hydrodynamic quantities in γ and β are evaluated without alpha particle energy deposition. Using Eqs. (7)–(8), both γ and β can be rewritten in terms of the shell areal density and hot spot temperature without alpha deposition. In one dimension, since both γ and β depends on areal density and temperature, the ignition parameter $\chi_{no\alpha}$ also depends on areal density and temperature. Note that with respect to the incompressible thin shell model of Ref. [7], the scaling of the ignition parameter is unchanged. A convenient form of χ is written in terms of areal density and neutron yield

$$\chi_{no\alpha} \simeq (\rho R_{no\alpha})^{0.61} \left(\frac{0.24 Y^{16}_{no\alpha}}{M^{\mathrm{unab}}_{\mathrm{DT}}} \right)^{0.34}, \qquad (11)$$

where ρR is in g/cm^2, yield in 10^{16} and the unablated DT mass in mg. Another form of $\chi_{no\alpha}$ is given in [7]

$$\chi_{no\alpha} \simeq (\rho R_{no\alpha})^{0.8} (T_{no\alpha}/4.7)^{1.6} YOC^{0.4}_{no\alpha}, \qquad (12)$$

where the temperature is in keV and the yield-over-clean $\mathrm{YOC} \equiv \mathrm{Yield(3D)/Yield(1D)}$ is a measure of the level of nonuniformities in the implosion. The model (1)–(5) is 1D but the same clean-volume analysis of Ref. [7] can be applied to capture 3D effects by redefining χ as in Eq. (12) by using the YOC or in Eq. (11) by using the measured yield. Note that Eq. (11) can be derived from Eq. (12) by using the approximate formula for the 1D yield $Y_{16}(1\mathrm{D}) = \rho R^{0.56}(T/4.7)^{4.7} M_{\mathrm{DT}}/0.24$ [7] into the YOC. The yield amplification due to alpha heating is computed by solving Eqs. (1)–(5) with $\gamma = 0$ (no alphas) and with a finite $\gamma < \gamma(\beta)$ (i.e., $\chi_{no\alpha} < 1$). The ratio of the resulting fusion yields [Yield$= \int_0^\infty \hat{P}^2 \hat{T} \hat{R}_h^3 d\tau$] represents the yield amplification. Figure 2(a) compares the yield amplification as a function of the ignition parameter obtained from hydrodynamic simulations with the curve from the alpha-heating model. The simulations are performed with the hydrocodes LILAC (1D) [14] and DRACO (2D) [15]. The results can be approximated with the fitting formula $\hat{Y}_{\mathrm{amp}} \approx (1 - \chi_{no\alpha}/0.96)^{-0.75}$. As stated in Ref. [7], the χ's from Eqs. (11), (12) are valid in three dimensions for relatively fast targets with $V_i \sim$ 300–400 km/s. Note that for a mass of DT of 0.18 mg, $\chi^{2.9}_{no\alpha}$ is approximately equal to the experimental

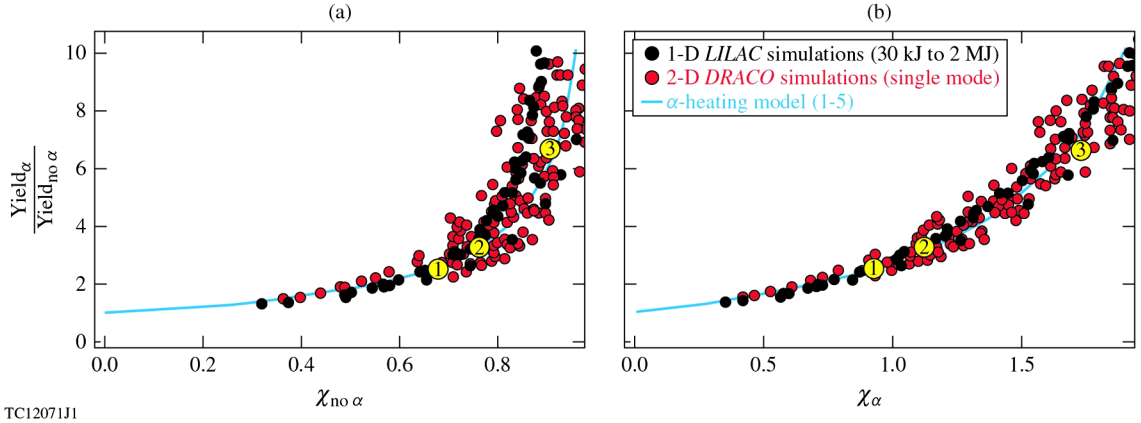

FIG. 2 (color online). Yield enhancement from alpha heating as a function of the alpha and no-alpha Lawson parameters using the model (1–5) (solid curve) and hydrodynamic simulations (dots). The measurable parameter χ_α can be used to determine the yield amplification from Fig. 2(b). Fig. 2(a) can be used to infer the no-alpha parameter $\chi_{no\alpha}$ which is useful for assessing progress toward ignition. Points 1–3 represent simulations with mass, adiabat and velocity similar to NIF ID targets (see Fig. 3).

ignition threshold factor parameter [16] (ITFx) for the Livermore indirect-drive ignition target [17] indicating that the validity of Eq. (11) as an ignition parameter is also confirmed by a large database of indirect-drive ignition-target simulations. In experiments with significant alpha heating, the $no\alpha$ quantities entering in the definition of $\chi_{no\alpha}$ cannot be directly measured. However, the measured yield and areal density can still be used into Eq. (11) to determine a value of χ with alphas (χ_α)

$$\chi_\alpha \simeq (\rho R_\alpha)^{0.61}\left(\frac{0.24 Y_\alpha^{16}}{M_{\rm DT}^{\rm unab}}\right)^{0.34}. \tag{13}$$

From Eqs. (1)–(5), a yield amplification curve using the measurable parameter χ_α is generated [Fig. 2(b)]. The yield amplification is approximately a unique function of χ_α, indicating that inferring χ_α from the experimental observables (ρR and yield), is sufficient to determine the yield amplification due to alpha heating in an experiment. Figure 2(b) compares the yield amplification versus χ_α from simulations with the alpha heating model (1)–(5). The model result can be approximated for amplifications $\lesssim 10$ with the simple formula $\hat{Y}_{\rm amp} \approx \exp(\chi_\alpha^{1.2})$. When compared to the results of Spears and Lindl [18] for the NIF indirect-drive ignition target ($M_{\rm DT} \approx 0.18$ mg), the yield amplification curves are in good agreement with the data points from the simulation database of that specific target. In Ref. [18], the Lawson parameter is computed from $P\tau/[P\tau]_{\rm ign}$ (related to χ as in Ref. [7]) with alpha deposition. In this Letter, the analysis is carried out in dimensionless form and the results are applicable to all targets, large or small, direct drive, or indirect drive as long as the ignition parameter χ_α is calculated using Eq. (13). For the high-foot shot N140120 [19], which achieved a yield of about 9.3×10^{15} neutrons, areal density of ≈ 0.78 g/cm^2, and ion temperature of 4.9 keV, with $M_{\rm DT} \approx 0.18$ mg, we find that $\chi_\alpha \approx 0.92$ and the yield amplification is ~ 2.5 (point 1 in Figs. 2) close to the simulation result [19]. The corresponding $\chi_{no\alpha} \simeq 0.66$ is inferred from Fig. 2 and the yield amplification.

The good agreement of the results from the alpha heating model and the hydrodynamic simulations (Fig. 2) indicate that the model can be used to determine the input energy to the fusing plasma and therefore the onset of the burning plasma regime. Energy is supplied to the DT plasma starting from the DT fuel kinetic energy $E_k(0) = 1/2 M_{\rm DT} V_i^2$, where 0 is the beginning of the deceleration phase. Only a fraction of the kinetic energy is transformed into DT internal energy through the pdV work. At bang time, the kinetic energy converted to internal energy is $E_{pdV}^{\rm tot} = E_k(0) - E_k(t_{\rm bang})$. Of that fraction, a portion is transferred to the dense shocked shell ($E_{pdV}^{\rm ss}$) and the other to the hot spot $E_{pdV}^{\rm HS}$. It is convenient to define two Q_α parameters, one for the hot spot and one for the entire compressed core,

$$Q_\alpha^{\rm HS} \equiv \frac{0.5 E_\alpha}{E_{pdV}^{\rm HS}}, \qquad Q_\alpha^{\rm tot} \equiv \frac{0.5 E_\alpha}{E_{pdV}^{\rm tot}}. \tag{14}$$

In these definitions, we retain the contribution of all the alpha particles up to bang time ($\sim 1/2$ of the total alpha energy) including those escaping. The ablative flow carries the escaping alpha energy back into the hot spot and such energy is counted as input to the hot spot. A value $Q_\alpha^{\rm HS} > 1$ implies that the alpha heating exceeds the compression work to the hot spot and the hot spot plasma enters the burning-plasma regime where the alpha heating is the dominant heating mechanism. Additional pdV work is done on the shell itself as the return shock propagates

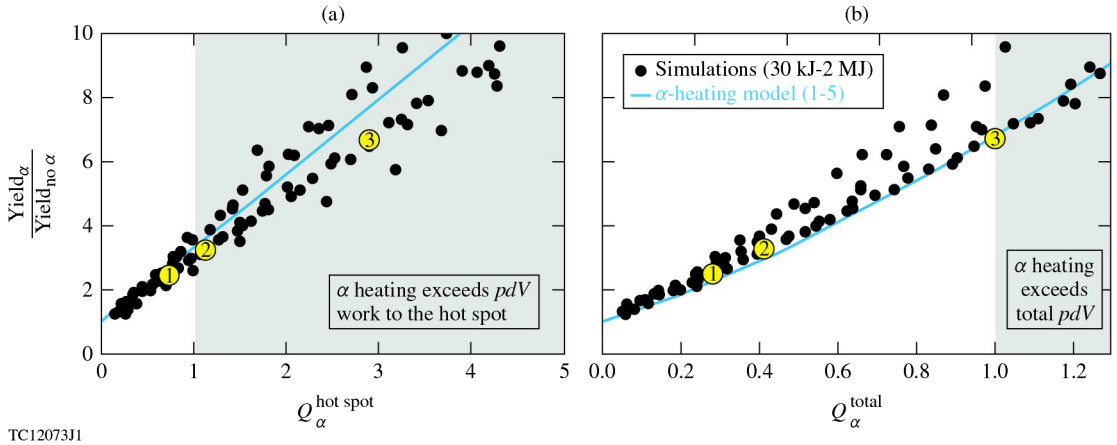

FIG. 3 (color online). Plots of the yield amplification versus the hot-spot Q_α (a) and the total Q_α (b) from the model (1–5) (solid curve) and from 1D simulations (dots). The shaded areas identify the burning plasma regimes. Points (1–3) with yield amplification $\sim 2.5\times$ (like shot N140120 [19]), $3.3\times, 6.7\times$ have fuel kinetic energy of ~ 12 kJ, adiabat $\lesssim 2$ and DT mass ≈ 0.18 mg like current NIF ID experiments. Point 2 is at the hot-spot burning-plasma onset. Point 3 is in the full burning plasma regime.

outward and more shell material is slowed down and compressed. While few fusion reactions occur in the dense shell at yield amplifications below 10, the compressed shell provides the inertial confinement to the hot spot pressure. The pdV work to the shell is not a direct input to the fusing plasma but a highly compressed shell increases the confinement time and therefore the fusion yield of the hot spot. In the second definition of Q_α, the total pdV work is included in the denominator and the condition $Q_\alpha^{\rm tot} > 1$ represents the regime where the alpha heating exceeds the total compression work. The pdV work to the hot spot can be calculated in one dimension from the integral $4\pi \int_{R(0)}^{R_{\rm stag}} PR^2 dR$, where $R_{\rm stag}$ is the hot-spot stagnation radius. Both quantities can be computed from the model (1)–(5) as well as from 1D hydrodynamic simulations of the implosions. In two or three dimensions, extracting the pdV work is more complicated and will be addressed in a forthcoming paper. Figure 3 shows the yield amplifications versus $Q_\alpha^{\rm HS}$ and $Q_\alpha^{\rm tot}$, and compare the result of the model (1)–(5) with hydrodynamic simulations. From Fig. 3(a), the onset of the hot-spot burning plasma regime occurs at yield amplifications of about 3.5. For current ID NIF implosions with $M_{\rm DT} \simeq 0.18$ mg, adiabat $\lesssim 2$, and fuel kinetic energies $\sim$12 kJ, this corresponds to a neutron yield of about 1.8×10^{16} (or $\sim$50 kJ) as indicated by the point 2 in Fig. 3(a). The regime where the alpha heating exceeds the total pdV work occurs for yield amplifications $\sim$7 corresponding to a yield $\sim 4.5 \times 10^{16}$ (or $\sim$120 kJ) represented by point 3 in Fig. 3(b). Shot N140120 [19] (point 1 in Fig. 3) has achieved $Q_\alpha^{\rm HS} \simeq 0.7$ and $Q_\alpha^{\rm tot} \simeq 0.28$. The measurable parameter χ_α can be used to determine the onset of the burning plasma regimes. Using Fig. 2, the hot-spot burning-plasma regime is achieved for $\chi_\alpha \approx 1.2$ while the full burning-plasma regime is achieved for $\chi_\alpha \approx 1.8$. The curves in Figs. 2–3 are used to assess the onset of the burning plasma regime in ICF and the requirements on the implosion hydrodynamics to achieve ignition. For instance, the value $\chi_{no\alpha} \approx 0.66$ for N140120 indicates that the $no\alpha$ hydrodynamics needs to improve to raise the value of $\chi_{no\alpha}$ by $\geq$50% to achieve ignition on NIF.

The authors thank Dr. J. Lindl, Dr. P. Patel, and Dr. D. Shvarts for many useful discussions. This work has been supported by the U.S. Department of Energy under Cooperative Agreements DE-FC02-04ER54789 (Office of Fusion Energy Sciences) and DE-NA0001944 (National Nuclear Security Administration), and by the New York State Energy Research and Development Authority.

[1] J. H. Nuckolls, L. Wood, A. Thiessen, and G. B. Zimmermann, Nature (London) **239**, 139 (1972).
[2] S. Atzeni and J. Meyer-ter-vehn, *The Physics of Inertial Fusion* (Clarendon, Oxford, 2004); J. D. Lindl, *Inertial Confinement Fusion* (Springer, New York, 1998).
[3] O. A. Hurricane, D. A. Callahan, D. T. Casey, P. M. Celliers, C. Cerjan, E. L. Dewald, T. R. Dittrich, T. Doppner, D. E. Hinkel, L. F. B. Hopkins *et al.*, Nature (London) **506**, 343 (2014).
[4] M. J. Edwards, P. K. Patel, J. D. Lindl, L. J. Atherton, S. H. Glenzer, S. W. Haan, J. D. Kilkenny, O. L. Landen, E. I. Moses, A. Nikroo *et al.*, Phys. Plasmas **20**, 070501 (2013).
[5] J. P. Freidberg, *Fusion Energy and Plasma Physics* (Cambridge University Press, Cambridge, England, 2007).
[6] J. D. Lawson, Proc. Phys. Soc. London Sect. B **70**, 6 (1957).
[7] P. Y. Chang, R. Betti, B. K. Spears, K. S. Anderson, J. Edwards, M. Fatenejad, J. D. Lindl, R. L. McCrory, R. Nora, and D. Shvarts, Phys. Rev. Lett. **104**, 135002 (2010); R. Betti, P. Y. Chang, B. K. Spears, K. S. Anderson, J. Edwards, M. Fatenejad, J. D. Lindl, R. L. McCrory, R. Nora, and D. Shvarts, Phys. Plasmas **17**, 058102 (2010).
[8] R. Betti, K. Anderson, V. N. Goncharov, R. L. McCrory, D. D. Meyerhofer, S. Skupsky, and R. P. J. Town, Phys. Plasmas **9**, 2277 (2002).
[9] A. Schiavi and S. Atzeni, Phys. Plasmas **14**, 070701 (2007).
[10] L. Spitzer, *Physics of Fully Ionized Gases* (Dover Publications, New York, 1956).
[11] S. X. Hu, L. A. Collins, T. R. Boehly, J. D. Kress, V. N. Goncharov, and S. Skupsky, Phys. Rev. E **89**, 043105 (2014).
[12] R. Kishony and D. Shvarts, Phys. Plasmas **8**, 4925 (2001).
[13] O. N. Krokhin and V. B. Rozanov, Sov. J. Quantum Electron. **2**, 118 (1973).
[14] J. Delettrez, R. Epstein, M. C. Richardson, P. A. Jaanimagi, and B. L. Henke, Phys. Rev. A **36**, 3926 (1987).
[15] P. B. Radha, T. J. B. Collins, J. A. Delettrez, Y. Elbaz, R. Epstein, V. Yu. Glebov, V. N. Goncharov, R. L. Keck, J. P. Knauer, J. A. Marozas *et al.*, Phys. Plasmas **12**, 056307 (2005).
[16] B. K. Spears, S. Glenzer, M. J. Edwards, S. Brandon, D. Clark, R. Town, C. Cerjan, R. Dylla-Spears, E. Mapoles, D. Munro *et al.*, Phys. Plasmas **19**, 056316 (2012).
[17] S. W. Haan, J. D. Lindl, D. A. Callahan, D. S. Clark, J. D. Salmonson, B. A. Hammel, L. J. Atherton, R. C. Cook, M. J. Edwards, S. Glenzer *et al.*, Phys. Plasmas **18**, 051001 (2011).
[18] J. D. Lindl, O. Landen, J. Edwards, E. Moses, and the NIC Team, Phys. Plasmas **21**, 020501 (2014); Phys. Plasmas **21**, 129902 (2014).
[19] O. A. Hurricane, D. A. Callahan, D. T. Casey, E. L. Dewald, T. R. Dittrich, T. Douppner, M. A. Barrios-Garcia, D. E. Hinkel, L. F. Berzak Hopkins, P. Kervin *et al.*, Lawrence Livermore National Laboratory, Report No. LLNL-JRNL-648209 (Appendix B), 2014.